NMR and Molecular Modeling Studies of the Interaction of Artificial AP Lyases with a DNA Duplex Containing an Apurinic Abasic Site Model†

Yannick Coppel, Jean-François Constant, Christian Coulombeau, Martine Demeunynck, Julian Garcia,* and Jean Lhomme

LEDSS, Chimie Bioorganique, UMR CNRS 5616, Université Joseph Fourier, BP 53, 38041 Grenoble Cedex 9, France

Received October 25, 1996; Revised Manuscript Received February 20, 1997⊗

ABSTRACT: Tailor-made molecules, DTAc and ATAc, that incorporate a nucleic base (adenine or 2,6-diaminopurine) linked by a diamino chain to an intercalator (9-amino-6-chloro-2-methoxyacridine) selectively recognize and efficiently cleave abasic sites in DNA *via* a β-elimination reaction. The three-dimensional structure of the complexes of DTAc and ATAc bound to a DNA undecamer, the $^{5'}d(C_1G_2C_3A_4C_5X_6C_7A_8C_9G_{10}C_{11})^{3'}\cdot{}^{3'}d(G_{22}C_{21}G_{20}T_{19}\ G_{18}T_{17}G_{16}T_{15}G_{14}C_{13}G_{12})^{5'}$ duplex in which the X residue is a stable abasic site [3-hydroxy-2-(hydroxymethyl)tetrahydrofuran], has been studied by combined NMR−energy minimization methods. Analysis of the NMR spectra reveals that DTAc and ATAc interact with a very similar fashion and form two different complexes with DNA, present in a ratio of 70/30 (±10). In both complexes, the acridine ring intercalates exclusively between the C3·G20 and A4·T19 base pairs, the linker is located in the minor groove, and the base moiety docks in the abasic site. The principal difference between the major and the minor complexes consists of a 180° rotation of the acridine ring around the Acr−C−N bond within the same intercalation site. Molecular modeling studies with few intermolecular ligand−DNA restraints were used to investigate the geometry of the base pair formed between the diaminopurine of DTAc and the T17 ring. The most energetically favored complex has the 2,6-diaminopurine of DTAc base paired with the T17 ring in a Hoogsteen conformation. The models DTAc and ATAc are also discussed as nuclease mimics and cleaving agents at abasic sites.

The loss of a nucleic base in DNA, i.e. formation of an abasic site, is one of the most frequent DNA lesions. This may occur through a variety of processes, either chemically—by protonation or alkylation of a purine base or by modification by physical agents such as radiation (Lindahl, 1993)—or enzymatically in the course of the repair of modified or abnormal bases (Loeb & Preston, 1986; Wallace, 1988; Lindahl, 1993; Demple & Harrison, 1994). The abasic site corresponds to a mixture of α- and β-hemiacetals in tautomeric equilibrium with the ring-opened aldehydic form which represents less than 1% of the total (Manoharan *et al.*, 1988a; Wilde *et al.*, 1989). Due to its noninformative character, the abasic lesion is mutagenic or lethal for the cell (Boiteux & Laval, 1982; Loeb & Preston, 1986). Its repair is thus a critical cellular activity. The first step of the repair process involves the action of specific nucleases that either hydrolyze the phosphodiester bond 5′ to the lesion (these are "true" AP[1] endonucleases that excise the abasic site as deoxyribose 5′-phosphate) (Demple & Harrison, 1994) or cleave the 3′ carbon−oxygen bond through a β-elimination mechanism that involves abstraction of the acidic proton α to the aldehydic group of the ring-opened form of the abasic site [these AP lyases generate an α,β-unsaturated aldose 5-phosphate (Bailly & Verly, 1989)]. The α,β-unsaturated aldose 5′-phosphate is then excised, and the resulting gap is repaired by a series of specific enzymes. The mechanism of β-elimination has been clearly demonstrated by NMR experiments on synthetic depurinated oligonucleotides (Manoharan *et al.*, 1988b; Mazunder *et al.*, 1991).

Some small chemical agents which can also cleave the AP site *in vitro* have been reported. Polyamines are the simplest ones (Male *et al.*, 1982). The tripeptide Lys-Trp-Lys (Behmoaras *et al.*, 1981; Pierre & Laval, 1981) and intercalating agents such as 9-aminoellipticine (Malvy *et al.*, 1986) or 3-aminocarbazole (Vasseur *et al.*, 1987) have also been shown to incise DNA at abasic sites at low doses. Their modes of action have been suggested to involve β-elimination, and formation of a Schiff base (path B in Scheme 1) between the aldehydic form of the AP site and an active amino group (Vasseur *et al.*, 1987).

Designing molecules that are able to selectively recognize the abasic site is a challenging fundamental problem that could be of practical interest for several reasons. Depending on the functional moieties that could be introduced into a basic "recognition system", new families of molecules possessing specific functions can be envisaged. These include AP endonuclease inhibitors, if binding to the abasic site is strong enough to allow the molecule to compete with

† This work was supported by the Association pour la Recherche sur le Cancer (ARC) and the Ligue Nationale contre le Cancer (LIGUE).

* Author to whom all correspondence should be addressed.

⊗ Abstract published in *Advance ACS Abstracts,* April 1, 1997.

[1] Abbreviations: AP, apurinic and apyrimidinic; DTAc, 9-[11-(6-chloro-2-methoxyacridin-9-yl)-3,7,11-triazaundecyl]-2,6-diamino-9*H*-purine hydrochloride; ATAc, 6-amino-9-[11-(6-chloro-2-methoxyacridin-9-yl)-3,7,11-triazaundecyl]-9*H*-purine hydrochloride; δppm, chemical shift in parts per million; EDTA, ethylenediaminetetraacetic acid; JUMNA, junction minimization of nucleic acids; NOE, nuclear Overhauser enhancement; NOESY, two-dimensional nuclear Overhauser enhancement experiment; DQFCOSY, double-quantum-filtered correlation spectroscopy; TOCSY, total homonuclear correlated spectroscopy; ROESY, two-dimensional rotating Overhauser enhancement experiment; rmsd, root mean square difference; SCF, self-consistent field.

S0006-2960(96)02678-5 CCC: $14.00

Scheme 1

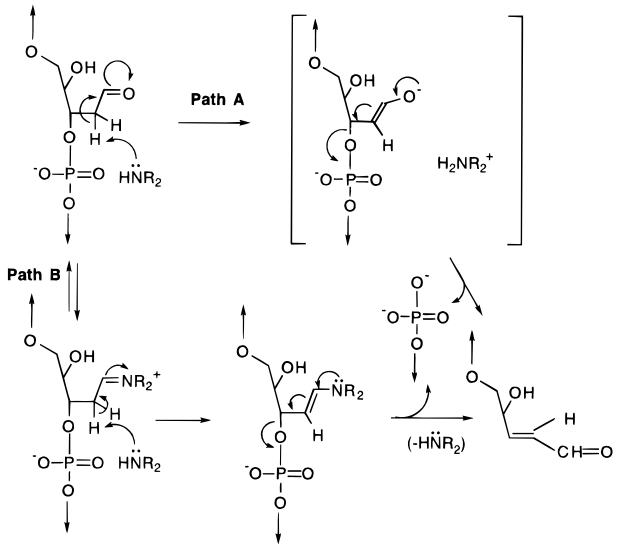

Scheme 2

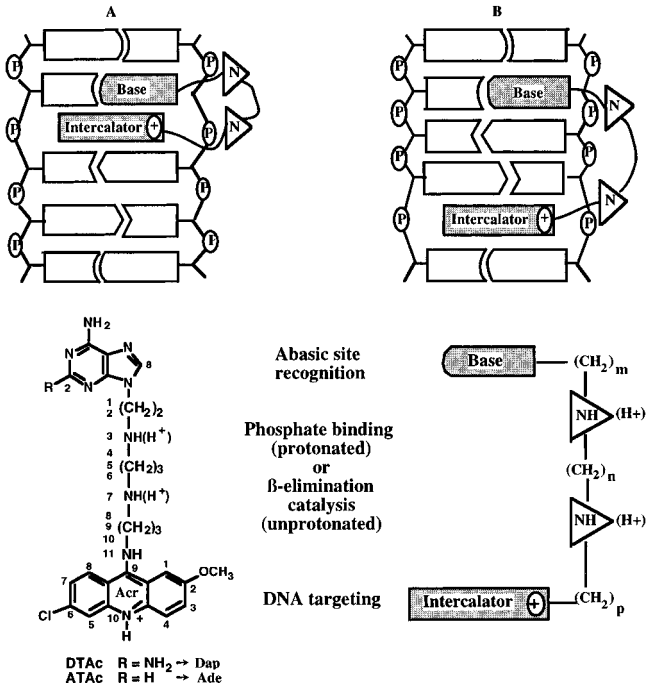

the enzyme, analytical probes for AP site analysis, if for example a fluorescent moiety is added to the recognition system, or nuclease mimics, if the molecules possess the catalytic functional group necessary for triggering cleavage. We have recently reported a number of results corresponding to the latter family, i.e., molecules that recognize and cleave abasic sites through β-elimination catalysis (Constant *et al.*, 1988, 1990; Fkyerat *et al.*, 1993a,b; Berthet *et al.*, 1994; Belmont *et al.*, 1996). The basic scheme for creating these tailor-made molecules is represented in Scheme 2. Such molecules include different structural units designed for specific functions: (1) an intercalator for targeting the molecule to DNA, (2) a nucleic base for recognition of the abasic site, and (3) a polyamino linker endowed with several functions, including an ionic binding function to the phosphates constituted by a protonated amino group in the chain, a cleavage catalysis function provided by a nonprotonated amino group, and a number of separating methylene groups, which control the pK_a's of the two amines (Belmont *et al.*, 1996) and determine the size of the molecule for fitting the abasic site locus. A number of molecules of this type have been prepared. The most efficient ones, i.e. DTAc and ATAc, have been shown to exhibit extreme cleavage efficiency, as they cleave pBR 322 plasmid DNA containing an average of 1.8 abasic sites per molecule at nanomolar concentrations of both partners (plasmid and cleaving agent) (Fkyerat *et al.*, 1993a). They are composed of a 9-amino-6-chloro-2-methoxyacridine intercalator linked by a diamino chain to the base diaminopurine (DTAc) or adenine (ATAc) (Scheme 2). These molecules exhibit a cleaving efficiency for apurinic sites in DNA which is much higher than that of the prototypical tripeptide Lys-Trp-Lys (Fkyerat *et al.*, 1993a). The three parts of the molecule, the base, the intercalator, and the chain, are necessary for the activity (Constant *et al.*, 1990). All cleavage results are in accordance with a mechanism involving a preorganized complex with DNA as indicated. Molecules that incorporate a strong intercalator, like the aminoacridine moiety, exhibit higher affinity for DNA and a higher cleavage efficiency than those incorporating the poor intercalator amino quinoline (Fkyerat *et al.*, 1993a). The diaminopurine moiety in DTAc increases both affinity and cleavage as compared to adenine in ATAc (Fkyerat *et al.*, 1993a). The presence of a linker devoid of amino functions leads to nonactive systems (i.e. a polymethylene chain or an amide-containing chain). In addition, the chemical nature of the termini of the DNA strand generated under the action of ATAc, as determined by enzymatic experiments, is in accordance with a β-elimination cleavage mechanism (Constant *et al.*, 1988).

Scheme 3

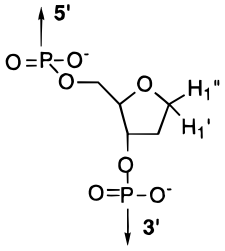

The "tetrahydrofuran analog" (X)

Although all the data collected favor Scheme 2, they are indirect results in terms of recognition of AP site DNA by either DTAc or ATAc. In order to obtain precise data concerning the nature and geometry of the complex(es), we undertook a high-field NMR study of the complex formed between molecules DTAc and ATAc and a synthetic DNA fragment containing an abasic site. For obvious stability reasons, we used the "classical" model abasic site, i.e., the 3-hydroxy-2-hydroxymethyltetrahydrofuran moiety replacing deoxyribose (Scheme 3) (Millican *et al.*, 1984; Takeshita *et al.*, 1987). The target oligonucleotide possesses the sequence indicated:

$$^{5'}d(C_1\ G_2\ C_3\ A_4\ C_5\ X_6\ C_7\ A_8\ C_9\ G_{10}\ C_{11})^{3'}$$

$$^{3'}d(G_{22}\ C_{21}\ G_{20}\ T_{19}\ G_{18}\ T_{17}\ G_{16}\ T_{15}\ G_{14}\ C_{13}\ G_{12})^{5'}$$

Thymine faces the abasic site, thus providing the complementary abasic site pocket for docking the adenine or the diaminopurine moiety of the synthetic molecules. The detailed conformation of this oligonucleotide is the object of the preceding paper (Coppel *et al.*, 1997). We observed in particular that the T17 thymine ring opposite the AP site

is stacked inside the helix, leaving a place for the base moieties of DTAc and ATAc. A kink of about 30° was observed for the helix at the site of the lesion.

We report here the solution structure of the complex(es) and show that the base inserts into the abasic pocket while the aminoacridine fragment intercalates at a distance of two base pairs.

MATERIALS AND METHODS

Sample Preparations. DTAc and ATAc and the abasic site-containing DNA undecamer were synthesized and purified as reported previously (Fkyerat *et al.*, 1993a; Coppel *et al.*, 1997).

The NMR samples were prepared by dissolving the undecamer in 650 μL of 99.96% D_2O containing 20 mM sodium phosphate buffer (pH 7.0), 0.1 M sodium chloride, and 0.1 mM EDTA. The concentration of the double-stranded DNA sample was 1.5 mM in 0.65 mL for NMR experiments.

Dilute stock solutions of DTAc and ATAc were prepared by dissolving about 1 mg in 200 μL of 99.96% D_2O. The concentrations of the stock solutions were measured by UV/visible absorbance with the extinction coefficient ϵ of 9430 M^{-1} cm^{-1} for DTAc and an ϵ of 8700 M^{-1} cm^{-1} for ATAc at 422 nm. The 1/1 drug−DNA complexes were prepared with the following procedure. Known amounts of DTAc and ATAc were added to the sample containing duplex DNA in ∼0.1 molar equiv per increment, and one-dimensional NMR spectra were recorded at each stage. A 1/1 complex was observed to have formed when resonances from the free oligonucleotide had been completely replaced by resonances from the complex.

A stock solution of DTAc was also kept at a temperature of 50 °C for 3 days in 99.8% D_2O in order to obtain the C8-deuterated molecule.

The complexes were then lyophilized three times and finally redissolved in 0.65 mL of 99.96% D_2O. For NMR experiments involving exchangeable protons, the oligomer was dissolved in 90% H_2O/10% D_2O.

NMR Experiments. NMR experiments were performed on a Varian Unity 600 spectrometer and on a Varian Unity *Plus* 500 spectrometer at temperatures of 1, 10, and 25 °C. Chemical shifts were referenced relative to the residual HOD resonance, which was previously calibrated to 3-(trimethylsilyl)propionate-2,2,3,3-d_4 (TSP-d_4). A set of two-dimensional NOESY (mixing times of 100, 250, and 400 ms), DQCOSY, TOCSY (mixing times of 40, 60, and 90 ms), ROESY (mixing time of 150 ms), and inversion recovery spectra were acquired in D_2O. NOESY spectra in 90% H_2O at 300 ms mixing times were recorded using the jump and return read pulse sequence. More details are provided in the previous study of the isolated undecamer (Coppel *et al.*, 1997).

Linear prediction was used to plot spectra. The first point in the F_2 dimension was corrected, and 212 points were added in the F_1 dimension.

Distance Restraints and Molecular Modeling. Intermolecular NOE cross-peaks were classified as strong, medium, and weak on the basis of visual inspection of the cross-peak intensities in the 250 ms NOESY spectra. A total of 16 intermolecular distance restraints were used. The intermolecular ligand−DNA restraints were set at 2.0−3.0, 2.0−4.0, and 2.0−5.0 Å for strong, medium, and weak NOEs, respectively. For methyl and methylene protons, 1 and 0.5 Å were respectively added to the upper bound of the restraint. Force constants of 12 and 6 kcal mol^{-1} for lower and upper bounds, respectively, were used.

Calculations were carried out and structures visualized on an IBM RS 6000-39H computer running JUMNA version 10 and Insight II version 95.0 (Biosym/Molecular Simulations). Modeling of the interaction of DTAc with the undecamer was performed using the JUMNA program package (Lavery *et al.*, 1995). DTAc was built using the Builder module of the Biosym Insight II software and was included in the JUMNA calculation with the help of the Nchem program. N3, N7, and Acr-N10 nitrogens were modeled as protonated groups with a total charge of +3.0 for DTAc. First partial charges were obtained by the Hückel−Del Re procedure of Nchem. Furthermore, to account for the conjugation of the Acr-C9−N11 bond, quadratic penalty terms with a force constant of 50 kcal mol^{-1} were used around this bond to maintain the coplanarity of the acridine moiety and the NH11−C10 group. The effects of water and counterions were simulated using a sigmoidal distance-dependent dielectric function and by reducing the charge on each phosphate group to −0.5e.

In the first step, the canonical B-form (Arnott *et al.*, 1980) of the DNA duplex was built using the JUMNA software and the intercalation site was created by imposing a rise of 6.8 Å and a twist of 20° either between the C3·G20 and A4·T19 base pairs or between the A8·T15 and C9·G14 base pairs. The abasic site is in the nucleotide library of the JUMNA software. DTAc was manually docked into the minor groove of the DNA duplex using the Insight II software.

After the first optimizations of the complex using the NMR restraints, the partial charges of DTAc were recalculated using an *ab initio* SCF single-point calculation in order to obtain more precise partial charges. This calculation was performed *in vacuo* using the Gaussian 94 system in the Hartree−Fock theory and the 3-21G* basis for the optimized conformation of DTAc. The optimizations of the complex were next made using these new charges for DTAc.

The protocol then used was described by Goulaouic *et al.* (1994). In the first stages, the helical variables and the sugar backbone variables of the DNA were locked. Minimizations were performed with gradual decreasing of the number of constraints until all variables were free to evolve. In all cases studied, i.e. for the different positions of the acridine moiety and for Hoogsteen or Watson−Crick base pairing between the base moiety of DTAc and the T17 residue, several starting positions were used. For each combination, only the lowest-energy conformation complex was considered and was subjected to stretching and twisting variations to ensure the stability of the local minima.

The final structures were analyzed with the programm CURVES version 5.0 (Lavery & Sklenar, 1990) which is especially well suited for the characterization of regular or irregular DNA features (Lavery & Sklenar, 1988, 1989).

RESULTS

The NMR assignments of the free DNA undecamer have been reported in the preceding paper (Coppel *et al.*, 1997). The proton resonances of the abasic site-containing DNA duplex in the complexes were assigned in a sequential manner using the well-established procedure developed for

Table 1: ^{1}H Chemical Shift Assignments and NOESY Cross-Peaks of DTAc in the Major 1/1 DTAc−DNA Complex[a]

proton	free	bound	$\Delta\delta$[b]	DTAc−DTAc NOEs[c]	DTAc−DNA NOEs[c]
Dap-H8	7.96	7.28	−0.68	CH_2-1 (m)	
CH_2-1	4.54	4.12	−0.42	CH_2-2 (s), Ade-H8 (m)	X6-H2′ (s), X6-H3′ (s)
CH_2-2	3.65	3.91	0.26	CH_2-1 (s)	X6-H2′ (m), X6-H3′ (m)
CH_2-4	3.39	na[d]			
CH_2-5	2.28	na			
CH_2-6	3.39	na			
CH_2-8	3.41	4.21	0.80	CH_2-9 (s)	G20-H4′ (m)
CH_2-9	2.51	4.11	1.60	CH_2-10 (s),CH_2-8 (s)	
CH_2-10	4.35	3.95	−0.40	CH_2-9 (s), Acr-H1 (w), Acr-H8 (m)	A4-H2 (m)
Acr-H1	7.68	7.10	−0.58	CH_2-10 (w), Acr-OMe (s)	
Acr-OMe	4.14	3.63	−0.51	Acr-H1 (s), Acr-H3 (s), Acr-H4 (w)	C3-H1′ (w), A4-H1′ (w), A4-H2 (w)
Acr-H3	7.75	6.26	−1.49	Acr-H4 (s), Acr-OMe (s)	C3-H2′ (w), C3-H6 (w)
Acr-H4	7.77	6.91	−0.86	Acr-H3 (s), Acr-OMe (w)	C3-H6 (w)
Acr-H5	7.82	7.27	−0.55		T19-Me (m)
Acr-H7	7.60	6.79	−0.81	Acr-H8 (s)	T19-H2″ (m), G20-H8 (w)
Acr-H8	8.37	7.37	−1.00	Acr-H7 (s), CH_2-10 (m)	G20-H1′ (m)

[a] H_2O is referenced at 4.97 ppm. Proton assignments are at 10 °C. [b] $\Delta\delta = \delta$(complex) − δ(DTAc). [c] s = strong, m = medium, and w = weak intensity. [d] Not assigned.

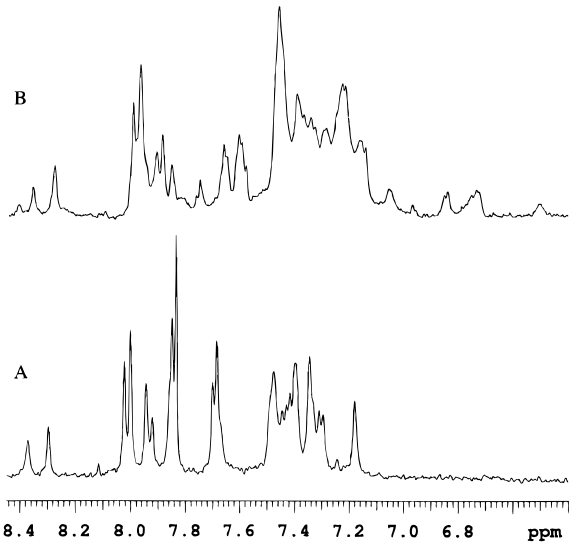

FIGURE 1: Aromatic regions of the one-dimensional NMR spectra of (A) d(CGCACXCACGC)·d(GCGTGTGTGCG) and (B) the 1/1 DTAc−d(CGCACXCACGC)·d(GCGTGTGTGCG) complex at 10 °C in 99.96% D_2O, 0.1 M NaCl, 20 mM sodium phosphate, and 0.1 mM EDTA at pH 7.0.

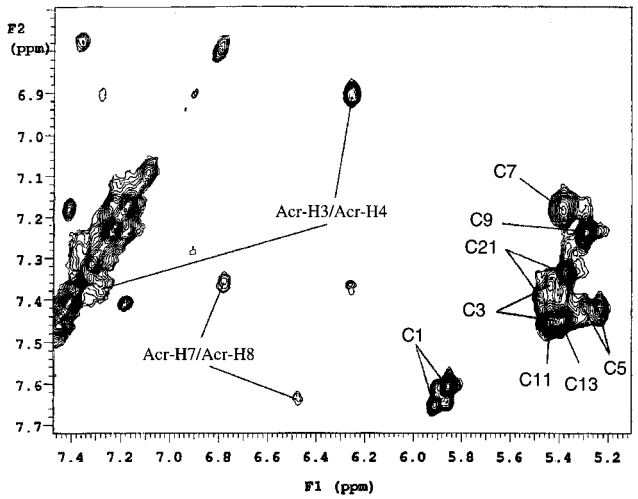

FIGURE 2: Aromatic region of the TOCSY spectrum (60 ms mixing time, 500 MHz) of the 1/1 DTAc−DNA complex in D_2O at 10 °C. Note the doubling of resonances for the C1, C3, C5, and C21 residues and for the acridine ring which illustrates the formation of two distinct complexes.

right-handed DNA duplexes (Feigon *et al.*, 1983; Scheek *et al.*, 1983; Wüthrich, 1986). This strategy is based on the relative proximity of the glycosidic protons (H1′, H2′, H2″, and H3′) to the base protons on the same residue and on their 3′-neighbor residues.

Proton Assignments of Free DTAc and ATAc. Due to the low solubility of DTAc and ATAc at pH 7.0, proton chemical shift assignments of free DTAc and ATAc were undertaken in 99.96% D_2O in the absence of sodium phosphate buffer at a concentration of ∼2 mM. The ATAc and DTAc protons were assigned unambiguously by a combination of 1 s NOESY and one-dimensional selective spin-decoupling experiments. These attributions are given in Tables 1 and S2 (Supporting Information) for DTAc and ATAc, respectively.

Characteristics of the Interaction of DTAc with the DNA Duplex. Figure 1 shows the aromatic region of the one-dimensional spectra of the DNA duplex in the absence and in the presence of 1 equiv of DTAc. The binding of the drug was demonstrated by the broadening of a number of DNA resonances. The 250 ms NOESY experiment, carried out in H_2O with a ratio of 1/2 DTAc−DNA, showed different sets of signals for the free and for the complexed DNA duplexes (data not shown). Additionally, no exchange peaks between these species could be observed. This implies a slow exchange between the free and the complexed DNA duplexes on the chemical shift time scale and on the relaxation time scale.

The NMR spectra of the 1/1 DTAc−DNA complex clearly showed the existence of two different complexes. That can be seen in the aromatic region of the 60 ms TOCSY spectrum shown in Figure 2. Two sets of cross-peaks were detected between Acr-H3 and Acr-H4 and between Acr-H7 and Acr-H8 protons. Furthermore, the same effect was observed for several DNA protons. It was particularly clear for the H6−H5 protons of the C1, C3, C5, and C21 residues that also displayed two sets of cross-peaks in the 60 ms TOCSY spectrum (Figure 2). Exchange peaks between these species were observed in 250 ms NOESY and in 150 ms ROESY carried out in D_2O (data not shown). This implies slow exchange between the two different 1/1 DTAc−DNA complexes on the chemical shift time scale, but with a rate constant greater than the exchange rate constant between free and complexed DNA duplexes. Some resonance lines of the DNA duplex at the binding site and of DTAc became broader when the temperature was increased (data not

Table 2: ^{1}H Chemical Shift Assignments of the DNA Resonances in the Major 1/1 DTAc−DNA Complex[a]

residue	H8	H6	H5/Me/H2	H1′	H2′	H2″	H3′	H4′	imino[b]	amino[c]
C1		7.61	5.86	5.74	1.92	2.37	4.70	4.08		8.19/7.05[e]
G2	7.92			5.79 (−0.14)	2.65	2.65 (−0.11)	4.99	4.34	12.87 (−0.26)	
C3		7.45	5.43	5.87 (0.20)	2.36 (0.29)	2.36	4.89	4.36 (0.14)		7.75/6.56 (−0.69/−0.03)
A4	8.39 (0.11)		7.19 (−0.63)	5.91 (−0.33)	2.57 (−0.12)	2.72 (−0.17)	4.99	4.43		
C5		7.44 (0.12)	5.24	5.33 (−0.59)	2.41 (0.21)	2.41 (0.21)	5.06 (0.20)	4.39 (0.18)		8.31/6.62 (0.21/0.05)
X6				4.18/4.02[d] (0.19/0.12)	2.28 (0.29)	2.28 (0.29)	4.73 (0.15)	4.20		
C7		7.19 (−0.47)	5.38 (−0.53)	5.34 (−0.22)	1.63 (−0.35)	2.23 (−0.17)	4.67 (−0.16)	4.25		8.36/6.53 (0.01/−0.46)
A8	8.28		7.59 (−0.25)	6.13	2.65 (−0.10)	2.85	4.98	4.38		7.92/6.10[e]
C9		7.25	5.29	5.59	1.91	2.30	4.81	4.15		8.23/6.70
G10	7.89			5.95	2.61	2.74	4.99	4.37	13.08	
C11		7.46	5.44 (0.13)	6.20	2.19	2.19	4.52	4.06		8.26/6.73[e]
G12	7.99			6.02	2.65	2.83	4.88	4.27	12.87[e]	
C13		7.45	5.39	5.79	2.22	2.51	4.91	4.25		8.47/6.62
G14	7.97			6.05	2.68	2.86	5.02	4.43	12.91	
T15		7.25	1.50	5.87	2.20 (0.30)	2.52 (0.26)	4.92	4.25	13.61 (−0.31)	
G16	7.87			5.94	2.57	2.75 (0.11)	4.98	4.36	12.87	
T17		7.32	1.29 (−0.29)	5.74 (−0.24)	2.28 (0.22)	2.48 (0.19)	4.90 (0.17)	4.27	na[f]	
G18	7.82 (−0.12)			5.90	2.54 (−0.17)	2.69 (−0.12)	4.99	4.36	12.07 (−0.66)	
T19		7.21 (−0.12)	1.47	5.83	2.29 (0.15)	2.29 (−0.21)	4.89	4.21	12.82 (−1.00)	
G20	7.96			5.89	2.71	2.71	4.89 (−0.11)	4.49 (0.10)	11.83 (−0.99)	
C21		7.34	5.37	5.74	1.91	2.33	4.83	4.22		8.29/6.60 (−0.21/−0.09)
G22	7.96			6.18	2.64	2.37	4.71	4.21	12.91[e]	

[a] H_2O is referenced at 4.97 ppm. Proton assignments are at 10 °C and pH 7 (at 600 MHz). Values in parentheses represent absolute values of chemical shift changes from free undecamer of ≥0.10 ppm [$\Delta\delta = \delta$(complex) − δ(DNA)]. [b] Assignments of H1 imino protons of guanine and of H3 imino protons of thymine. [c] Assignments of hydrogen-bonded amino protons and exposed amino protons of cytosine. [d] Assignments of H1′ and H1″ protons of the abasic site. [e] Assigned at 1 °C. [f] Not assigned.

shown), suggesting that the exchange dynamics of the different complexes is in the intermediate to slow exchange rate range on the chemical shift time scale.

The proportion between the two complexes at 10 °C was established by integrating and comparing the cross-peak volumes of Acr-H3 and Acr-H4, Acr-H7 and Acr-H8, C1-H6 and C1-H5, and C5-H6 and C5-H5 protons in the 60 ms TOCSY experiment. The approximate ratio of the two complexes is 70/30 with a precision of ±10%. Due to the broadening of the proton resonances, the presence of other complexes which could represent, at the most, less than 10% of the total cannot be excluded.

Nonexchangeable Proton Assignments for the Major 1/1 DTAc−DNA Complex. The proton assignments of DTAc in the major 1/1 DTAc−DNA complex were made by analysis of DQCOSY, TOCSY, and NOESY spectra. They are listed in Table 1. The Acr-H1 proton of the acridine moiety was identified from its NOEs with the CH_2-10 and the Acr-OMe protons. The Acr-H3 and Acr-H4 protons were assigned on the basis of their coupling constant (≈9.0 Hz) and from the Acr-H3 NOE with the Acr-OMe. The Acr-H7 and Acr-H8 protons were also assigned on the basis of their coupling constant and from the Acr-H8 NOEs with the CH_2-10 protons. The Acr-H5 was assigned on the basis of its weak coupling constant (≈2.0 Hz) with the Acr-H7 proton. Compared to the free state of DTAc, the acridine proton resonances are moved upfield by as much as 0.5 ppm. These shifts are consistent with a structure in which the acridine ring system stacks between the DNA base pairs. Furthermore, the data indicate preferential shielding of the Acr-H3, Acr-H4, Acr-H7, and Acr-H8 protons.

The CH_2-8, CH_2-9, and CH_2-10 protons of the linker were assigned by observing dipolar and scalar mutual connectivities and by NOE connectivities between the CH_2-10 protons and the Acr-H1 and Acr-H8 protons. The CH_2-4, CH_2-5, and CH_2-6 protons could not be unambiguously assigned. The Dap-H8 proton was identified by exchange experiments in which this proton was replaced by deuterium and the spectra of the corresponding complex were recorded (Figure S1, Supporting Information). The CH_2-1 proton resonances were assigned from NOEs with the Dap-H8 and with the CH_2-2 protons and confirmed by observing DQCOSY connectivities between the two methylene protons.

The 250 ms NOESY spectrum performed in D_2O was primarily used to make the assignments of the DNA protons. These were confirmed by a more detailed examination of the cross-peaks in the DQCOSY, TOCSY, and 100 ms NOESY spectra. The A8-H2 proton unlike the A4-H2 proton was readily distinguished from the other base protons in a one-dimensional inversion−recovery experiment (data not shown).

The proton resonances of the tetrahydrofuran moiety of the AP site were readily assigned from the NOESY and DQCOSY spectra. The abasic H1′/H1″ protons resonating at 4.17 and 4.02 ppm, respectively, were distinguished on the basis of cross-peak intensities between the abasic H1′/H1″ protons and abasic H3′ proton in the 100 ms NOESY spectra. Peak assignments of the major 1/1 DTAc−DNA complex are listed in Table 2.

In the AP site-containing strand, two breaks in the NOE connectivities were detected between the C5 and X6 residues, due to the absence of any base proton at the abasic site, and between the C3 and A4 residues. In the opposite strand, a break was also detected between the T19 and G20 residues. The break between base pairs C3·G20 and A4·T19 is explained by the intercalation of acridine at this site.

The undecamer can be separated into two domains. The first one, designated as the "5′-part" relative to the position with respect to the AP site, comprises base pairs C1·G22−C5·G18. The second, designated as the "3′-part", comprises

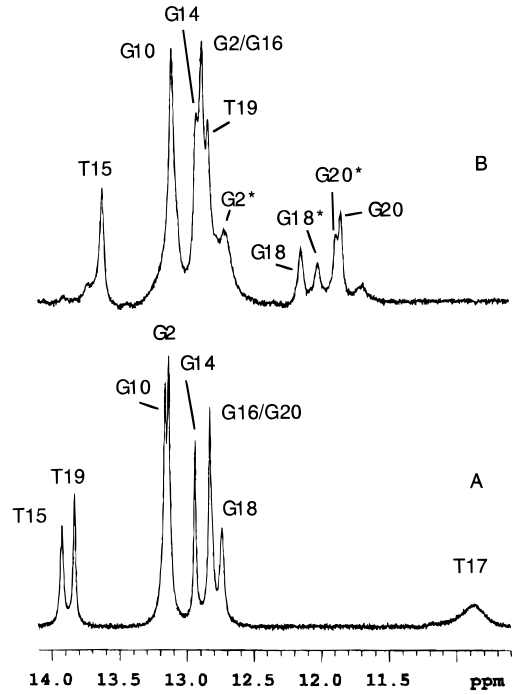

FIGURE 3: Imino proton spectra at 600 MHz of (A) d(CGCACXCACGC)·d(GCGTGTGTGCG) and (B) the 1/1 DTAc−d(CGCACXCACGC)·d(GCGTGTGTGCG) complex in H_2O at 10 °C. Resonances due to the minor complexes are marked with asterisks. Note the upfield shifts of the imino protons of the G18 and G20 residues and the displacement of the T19 imino proton resonance.

base pairs C7·G16− C11·G12. The pattern and the relative intensities of the cross-peaks between the base protons and the H1′, H2′, and H2″ protons for the nucleotides of the 3′-part indicate that this region forms a regular right-handed structure. On the other hand, the DNA peaks of the nucleotides belonging to the 5′-part appear to be broadened. The degree of line broadening for the C3, A4, T19, and G20 residues is very important and confirms the presence of competing complexes. Comparison of the chemical shifts in the complexed and the uncomplexed oligomers showed that the largest changes in the chemical shifts relative to the free undecamer (Table 2) occur at the C3·G20, A4·T19, C5·-G18, X6·T17, and C7·G16 nucleotides (from −0.63 to 0.29 ppm).

Exchangeable Proton Assignments for the Major 1/1 DTAc−DNA Complex. Figure 3 shows the imino region of the one-dimensional spectra of the DNA duplex in the absence and the presence of 1 equiv of DTAc. The exchangeable imino and amino protons were assigned using their dipolar connectivities in two-dimensional NOESY spectra recorded at 1 and 10 °C. They are given in Table 1. Cross-peaks can be observed between the thymine imino N3H protons and the adenine H2 protons in the A4·T19 and A8·T15 base pairs. These attributions were confirmed by observing weak cross-peaks between the imino N3H protons and their corresponding methyl protons. As observed for the nonexchangeable protons, the correlations involving the protons of the A4·T19 base pair are particulary weak, probably reflecting the equilibrium between the different competing complexes. The guanine imino protons were identified through their characteristic NOEs with the hydrogen-bonded and with the exposed cytidine amino protons which also display NOEs with the nonexchangeable H5 cytosine protons. These cross-peaks are consistent with Watson−Crick base pairing.

The T19 imino proton (12.82 ppm) and G20 imino proton (11.83 ppm) shifted upfield by ∼1 ppm relative to their chemical shifts in the free DNA. This assignment is in agreement with preferential intercalation of the acridine ring between base pairs C3·G20 and A4·T19. The G18 imino proton (12.07 ppm) also showed a broad resonance and shifted upfield by ∼0.7 ppm relative to the chemical shift in the free DNA.

The chemical shift of the T17 imino proton was observed at 10.86 ppm in the free undecamer. This signal was absent in the bound undecamer, and the T17 imino proton could not be assigned, even by an NMR experiment monitored at 1 °C or by comparison of NMR experiments with the C8H or the C8^{2}H DTAc. None of the exchangeable protons of the drug were observable.

In order to monitor the effect of the molecule DTAc on the stability of the duplex, the line width of the imino protons as a function of temperature was followed. The imino protons were totally absent at a temperature of 65 °C. This value is approximately 15 °C higher than that observed for the abasic DNA duplex in the absence of the drug (Coppel *et al.*, 1997).

Intermolecular NOE Contacts in the Major 1/1 DTAc−DNA Duplex. The analysis of the NOESY spectra of the complex showed several cross-peaks between the drug and the DNA protons (Table 1).

The position of the acridine dye was determined through the intermolecular dipolar contacts of its aromatic protons with certain C3, A4, T19, and G20 protons (Figure 4). These NOEs are consistent with intercalation of the acridine moiety between the C3·G20 and A4·T19 base pairs and allowed the determination of the orientation of acridine. The H2′/H2″ proton resonance overlap of C3, X6, and T19 makes attribution of the H2′ or H2″ NOEs difficult. Their relative contributions were estimated from the first models obtained with the remaining restraints. However, to take account of spin diffusion, 0.5 Å was added to the upper bound of the restraints for these NOEs.

In addition, NOE contacts were observed between the CH_2-10 linker protons and the A4-H2 proton and between the CH_2-8 linker protons and the G20-H4′ proton, positioning the polyamino linker in the minor groove of the duplex. No dipolar connectivity could be observed between the Dap-H8 proton of DTAc and the nonexchangeable protons of the oligonucleotide. However, some NOE contacts were observed between the CH_2-1 and CH_2-2 linker protons and the abasic sugar protons (Figure 4), positioning the base moiety of DTAc at the abasic site.

Determination of the Minor 1/1 DTAc−DNA Complex. It was not possible to detect intermolecular NOE connectivities or to follow the sequential connectivites in the minor DTAc−DNA complex due to its low abundance and to the important line width of the resonances at the binding site. However, the acridine protons could be assigned, and their chemical shifts were also in agreement with intercalation of the acridine ring between the DNA base pairs (Table S1, Supporting Information).

The chemical shifts of the DNA protons appeared to be very similar in both complexes as can be seen for the exchangeable proton resonances, especially those corresponding to the T19 and G20 imino protons. It can thus be estimated that the conformation of the minor 1/1 DTAc−DNA complex is nearly identical to the major 1/1 DTAc−DNA complex, the difference presumably arising from the

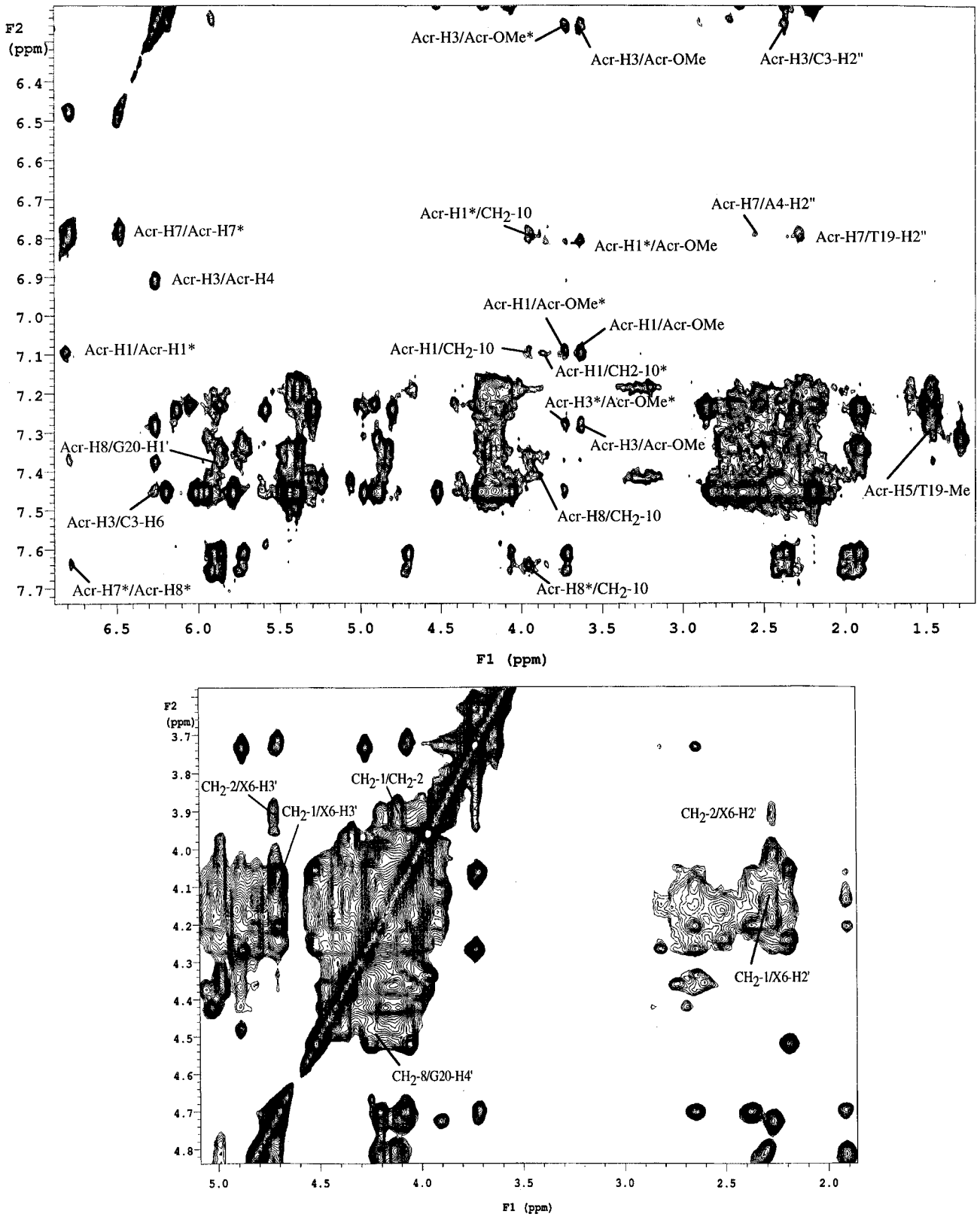

FIGURE 4: Expanded NOESY (250 ms mixing time, 500 MHz) of the 1/1 DTAc−DNA complex in D_2O at 10 °C in 0.1 M NaCl, 20 mM sodium phosphate, and 0.1 mM EDTA at pH 7.0 dissolved in 99.96% D_2O. Selection of intermolecular drug−DNA and intramolecular drug−drug cross-peaks. Resonances due to the minor complexes are marked by asterisks.

orientation of the acridine ring in the two complexes. Furthermore, several acridine protons show NOE connectivities with DNA protons of both strands. The most significant example arises from the Acr-H7 proton which has a medium-intensity NOE with the T19-H2″ proton and two weak-intensity NOEs with the A4-H2′ and C3-H2″ protons. These connectivities cannot exist simultaneously with the unique position of the acridine moiety, and we conclude that the acridine ring resides in two positions, which differ by a 180° rotation of the acridine plane around the Acr-C9−N11 bond. These connectivities are typical of an intermediate to fast exchange between the competing complexes on the relaxation time scale, and similar effects are observed for several DNA protons at the binding site.

Characterization of the Interaction of ATAc with the DNA Duplex. In the NMR spectra, the ATAc−DNA complex clearly showed the same behavior as the DTAc−DNA complex (Figures S2−S4, Supporting Information). We also observed two complexes in equilibrium in approximately the same proportions as that for the 1/1 DTAc−DNA complex. The internuclear NOE patterns between the DNA and the ligand protons and the proton chemical shifts are very similar for both the DTAc and the ATAc complexes. It can thus be concluded that the structures of the 1/1 ATAc−DNA complexes are close to those of the 1/1 DTAc−DNA complexes. However, the line widths of the resonances of the DNA protons at the binding site appeared to be broader for the 1/1 ATAc−DNA complexes. Due to the broadening of the resonances, the proton assignment for the major 1/1 ATAc−DNA complex appeared to be more problematic and the NOE contacts between the drug and DNA observed were less clear. The proton assignment was greatly aided by comparison with the results obtained for the major 1/1 DTAc−DNA complex. The chemical shifts of the protons of the molecule ATAc and of the duplex in the major 1/1 ATAc−DNA complex are given in Tables S2 and S3 (Supporting Information), respectively. The Ade-H2 and Ade-H8 protons could not be assigned. Table S2 also displays the intermolecular NOEs observed between the protons of ATAc and the DNA duplex.

Several protons near the abasic site exhibit two sets of broad resonances showing that the position of the drug base is not as well-defined as in the 1/1 DTAc−DNA complexes. Another difference also appears in the chemical shift values for the H6 proton of the T17 residue in the major complexes which is 7.32 ppm in the 1/1 DTAc−DNA complex and 7.20 ppm in the 1/1 ATAc−DNA complex. This observation could indicate a slight difference in the T17 geometry with each of the two drugs.

DISCUSSION

All these collected data allow a clear description of the complexes formed between the two drugs DTAc and ATAc and the abasic site-containing undecamer. The main observations can be summarized as follows.

Multiple Conformations and Sequence Selectivity. The NMR data indicate that both molecules DTAc and ATAc form two different competing intercalation complexes with the abasic site-containing undecamer. These complexes are present approximately in a 70/30 (±10%) ratio and are in slow to intermediate exchange on the chemical shift time scale. The NMR experiments also reveal that the molecules DTAc and ATAc bind exclusively in the C3·G20−C7·G16 region of the DNA duplex. This is supported by the fact that the greatest DNA proton chemical shifts differences were observed in this region. Furthermore, the line broadening of the protons in this region confirms the presence of several competing complexes.

Intercalation of the Acridine Moiety between the C3·G20 and A4·T19 Base Pairs. The NMR spectra of the major complexes of 1/1 DTAc−DNA and ATAc−DNA provide clear evidence for intercalation of the acridine moiety between the C3·G20 and A4·T19 base pairs. In each complex, the T19 and G20 imino protons are shifted upfield by ∼1.0 ppm (Table 2) relative to their chemical shift in the free DNA. Upfield chemical shift differences between free and bound molecules are observed for all acridine protons of DTAc and ATAc and are in the range of 0.5−1.49 ppm (Table 1), indicating intercalative binding of the drug. The position of the intercalation site is confirmed by the interruption of the sequential connectivities between the C3 and A4 and T19 and G20 residues and by the presence of NOE contacts between acridine protons and C3, A4, T19, and G20 protons (Table 1). The orientation of the acridine moiety is well-defined by these NOEs.

The NMR data also show some evidence that the acridine moiety in the minor complexes is also intercalated between the same C3·G20 and A4·T19 base pairs. The chemical shifts of the DNA protons are nearly identical in the two complexes, and the acridine protons are typical of intercalation of the acridine rings in the duplex (Table S1, Supporting Information). Some acridine protons of DTAc and ATAc also have NOE contacts with DNA protons of both strands of the intercalation site. These signals can be tentatively explained by the existence of an equilibrium between two acridine positions which differ by a 180° rotation of the acridine moiety around the Acr-C9−N11 bond and indicate an exchange faster than the NOE growth.

Minor Groove Binding. The acridine ring intercalates *via* the minor groove as shown by the NOEs between the CH_2-10 and the A4-H2 protons and between the CH_2-8 and the G20-H4′ protons. Several NOE cross-peaks enabled us to determine the position of the acridine ring and allowed us to unambiguously position the linker in the minor groove. As a result of minor groove binding, induced chemical shift differences relative to the free undecamer for H1′, H2′, and H2″ protons located at the binding site level are among the most important (Table 2).

Docking of the Base Moiety of DTAc and ATAc into the Abasic Pocket. The NMR results indicate that the diaminopurine moiety of DTAc and the adenine moiety of ATAc insert into the abasic pocket. This is shown by the C7-H6 and -H5 protons that are shifted upfield by ∼0.5 ppm relative to their position in the free undecamer. These large differences can only be explained by the presence of an aromatic ring stacked upon the cytosine ring. It is interesting to note that in the free undecamer the C7 base protons display chemical shifts nearly identical to those of the C1, due to the absence of a 5′-stacked base, whereas in the complex, these C7 base protons display chemical shifts close to those of cytosines possessing a 5′-stacked neighbor. NOEs observed between the CH_2-1 and the CH_2-2 protons and the H3′ and H2′/H2″ protons of the X6 residue also confirm that the base moieties of DTAc and ATAc are located in the abasic site.

The T17 imino resonance line in the complex could not be unambiguously assigned. This resonance is probably shifted relative to the free undecamer which could tentatively be explained by the formation of a hydrogen bond between this proton and a heteroatom of the base moiety of DTAc and ATAc. However, the NMR data alone do not enable us to determine how the diaminopurine moiety of DTAc or the adenine moiety of ATAc is base-paired with the T17 residue.

Conformation of the Major 1/1 DTAc−DNA Complexes. Molecular modeling studies of the DTAc abasic site-containing undecamer complex were carried out using the JUMNA software. Due to the presence of competing complexes and because of the few intermolecular NOEs available, it was not possible to make a quantitative study of the DTAc−DNA complex. However, molecular modeling

was used to investigate the geometry of the base pair formed between the diaminopurine moiety of DTAc and the T17 residue and to try to distinguish between the possible Hoogsteen or Watson−Crick conformations. Representative starting structures for both conformations were generated by positioning the acridine ring between the C3·G20 and A4·T19 base pairs in an orientation consistent with the observed NOE contacts, by docking the linker into the minor groove, and by positioning the diaminopurine into the abasic pocket in an orientation consistent with the Hoogsteen or Watson−Crick conformation. These structures were submitted to the protocol described in Materials and Methods.

Figure 5 shows the two best energy-minimized structures for each conformation, and their various energy contributions are summarized in Table 3. These model structures satisfy all the NOE restraints to within 0.2 Å.

The acridine orientation in both models is very similar. The long axis of the acridine ring is approximately parallel to the long axis of the C3·G20 and A4·T19 base pairs with the chloro and the methoxy groups located in the major and in the minor grooves, respectively (Figure 6). Detailed inspection of the two models reveals that the amino protons of the linker make several hydrogen bonds with DNA. For the Hoogsteen conformation, hydrogen bonds are observed between NH_2-3 and the C5-O2 (1.96 Å) and between NH_2-7 and one oxygen of the T19 phosphate group (2.27 Å). For the Watson−Crick conformation, hydrogen bonds are observed between NH_2-3 and C5-O3′ (2.16 Å), between NH_2-3 and the X6-O4′ (1.98 Å), between NH_2-7 and T19-O2 (2.48 Å), and between NH_2-7 and one oxygen of the T19 phosphate group (1.73 Å). Furthermore, other electrostatic interactions between the positive NH_2-3 and NH_2-7 groups of DTAc and the negative phosphate groups of the C5 and the T19 residues, respectively, significantly contribute to stabilization of both complexes. The diaminopurine moiety of DTAc can also form several hydrogen bonds with DNA. For the Hoogsteen conformation, hydrogen bonds are observed between Dap-NH_2-4 and T17-O4 (2.07 Å), between Dap-N7 and T17-NH3 (2.00 Å), and between Dap-NH_2-2 and one oxygen of the C5 phosphate group (2.05 Å). For the Watson−Crick conformation, hydrogen bonds are observed between Dap-NH_2-4 and T17-O4 (2.01 Å), between Dap-N3 and T17-NH3 (2.03 Å), and between Dap-NH_2-2 and T17-O2 (1.89 Å). Steric clashes between the abasic site-containing strand and the diaminopurine are more important in the Watson−Crick than in the Hoogsteen conformation, resulting in a better stacking of the diaminopurine moiety with the C7 ring in the Hoogsteen conformation (Figure 6).

The DNA duplex in the two models shows characteristics of the B-form-like DNA conformation with similar structural features (rmsd for heavy atoms is 1.6 Å) except for the T17 residue (Figure S5, Supporting Information). In the two models, the abasic sugar is pushed out into the minor groove (Figures 5 and 7) and the T17 residue remains within the helix as was observed in the NMR experiments. The conformation of the T17 base exhibits more perturbations relative to standard B-DNA in the Watson−Crick conformation than in the Hoogsteen conformation (roll value of −15.7 and 5.1° for the Watson−Crick and the Hoogsteen conformations, respectively). Furthermore, the T17 residue is less stacked with G16 in the Watson−Crick conformation than in the Hoogsteen conformation (shift value of −1.9 and 0.1 for the G16/T17 step, respectively) due to the base pairing with the diaminopurine moiety (Figure 7).

The Hoogsteen conformation is prefered over the Watson−Crick conformation by 17.1 kcal mol^{-1} (Table 3). The overall energy difference between the two models principally arises from the ligand energy contribution showing that DTAc in the Watson−Crick conformation cannot optimize its geometry as well as in the Hoogsteen conformation. Detailed inspection of the various contributions of the DTAc−DNA energy interaction also reveals some differences between the two models. The Hoogsteen conformation shows a higher van der Waals component due to better stacking of the diaminopurine moiety with the C7 residue. The Watson−Crick conformation shows a higher electrostatic component due to the formation of three hydrogen bonds between the diaminopurine moiety and the T17 residue, versus two hydrogen bonds for the Hoogsteen conformation. However, this difference is reduced by the formation of a hydrogen bond between Dap-NH_2-2 and one oxygen of the C5 phosphate group in the Hoogsteen conformation.

Furthermore, the NMR data are better fitted by the Hoogsteen conformation than by the Watson−Crick conformation; no NOE contacts, as expected for the Watson−Crick conformation, could be detected between the Dap-H8 proton and the C5-H1′ (4.73 Å), -H2′ (4.19 Å), and -H2″ protons (3.01 Å) and between Dap-H8 and the C7-H5 proton (4.13 Å). The C7-H6 and -H5 chemical shift differences relative to those in the free undecamer also seem to be better represented by the Hoogsteen conformation, as predicted by theoretical calculations of the shielding effect of the adenine ring (Giessner-Pettre & Pullman, 1976) extrapolated to the diaminopurine ring. However, NMR evidence and molecular modeling are not sufficiently clear to completely exclude the Watson−Crick conformation.

Conformation of the Minor 1/1 DTAc−DNA Complex. The minor 1/1 DTAc−DNA complex shows similarities with the major 1/1 DTAc−DNA complex. To obtain a model of the minor complex, we made molecular mechanics calculations starting from the best Hoogsteen conformation model in which the acridine ring was rotated by 180° relative to the Acr-C9−N11 bond. The final structure is represented in Figure S6 (Supporting Information). The long axis of the acridine ring in this model is more perpendicular to the long axis of the C3·G20 and A4·T19 base pairs than in the major complex. This model seems to be in reasonable agreement with the observation that the Acr-H7 proton can give NOEs with the C3-H2″ (4.40 Å) and the A4-H2′ (4.92 Å) protons.

Intercalation of Acridine 5′ versus 3′ to the Abasic Site. We also used molecular modeling to understand why the acridine ring does not intercalate between the A8·T15 and C9·G14 base pairs. The orientation of the linking chain in the 3′-direction relative to the abasic site creates a crowding between the drug linker and the abasic site-containing strand which prevents the formation of the base pairing between the diaminopurine moiety (Figure S7, Supporting Information) and T17 and perturbs formation of hydrogen bonds beetween the linker and DNA. These steric hindrances are due to the orientation of the Dap-N9−C1 bond which points toward the AP site-containing strand in both the Hoogsteen and the Watson−Crick conformations.

Comparison between DTAc and ATAc Complexation with the Abasic Duplex. It has been shown that substitutions of adenine by diaminopurine in deoxyribonucleotides increase their melting temperature (Chollet & Kawashima, 1988; Chazin *et al.*, 1991). It thus seems reasonable to assume

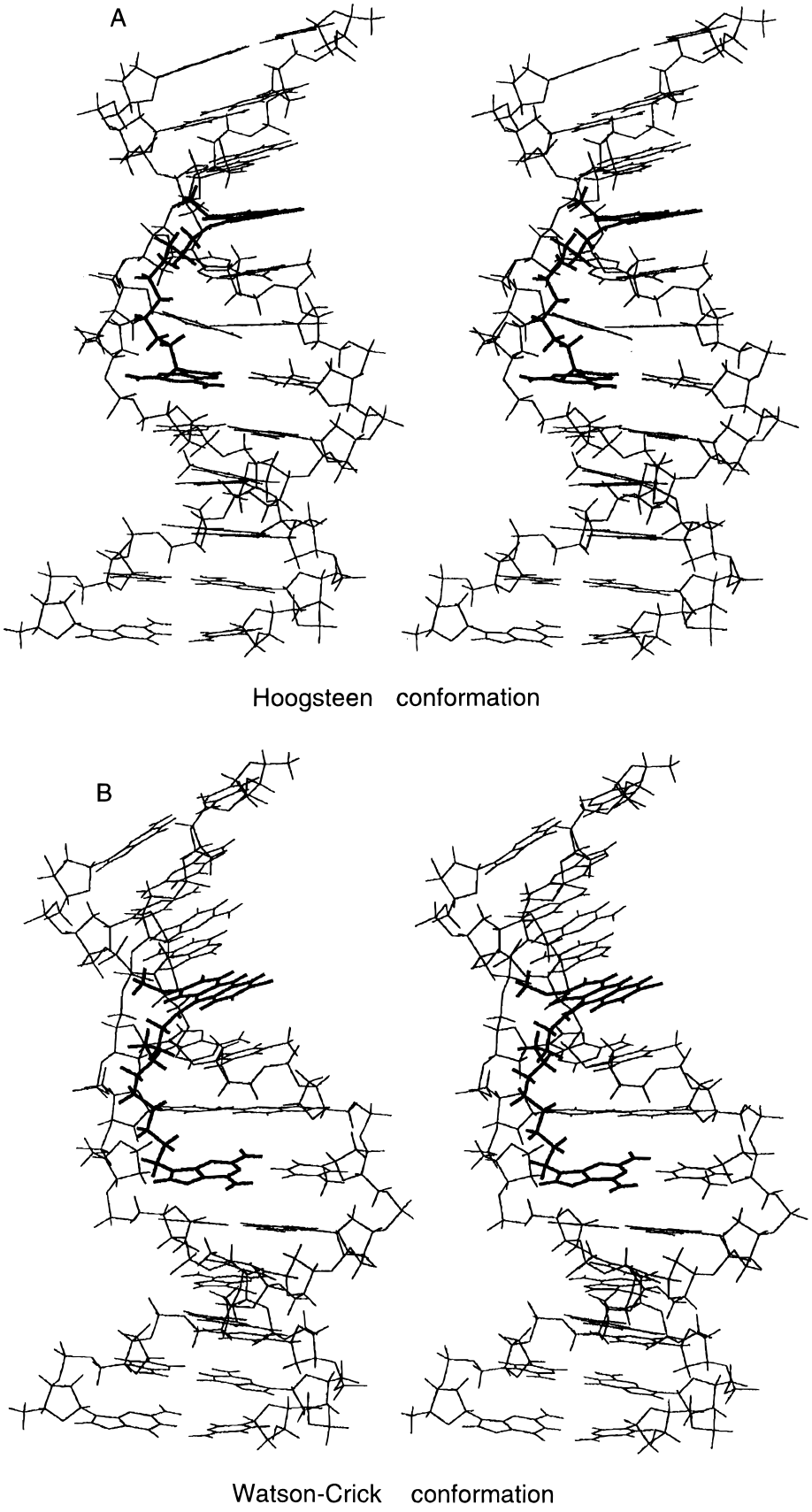

FIGURE 5: Stereoview of the model for the major 1/1 DTAc−DNA complex with (A) the Hoogsteen conformation and (B) the Watson−Crick conformation. DTAc is shown in bold lines.

that DTAc shows a stronger association with the abasic site-containing undecamer, which could explain why this complex led to a better defined NMR spectra. However, the DTAc−DNA and ATAc−DNA complexes seem very similar. The only differences consist of slight geometric changes for the drug base, for T17 and for the adjacent residues due to the presence of the supplementary hydrogen bond donor NH_2-2 amino group in the diaminopurine species. Molecular modeling computations of the major 1/1 ATAc−DNA complex were undertaken by starting from the optimized

Table 3: Energetic Terms (Kilocalories per Mole) of the Major 1/1 DTAc−DNA Complex

			$E_{DTAc-DNA}$[c]			
model	E_{DNA}[a]	E_{DTAc}[b]	vdw	elec	total	$E_{complex}$[d]
Hoogsteen	−513.2	231.3	−74.3	−135.9	−210.1	−511.0
Watson−Crick	−516.6	212.3	−68.7	−140.0	−208.6	−493.9

[a] Total energy of the DNA in the complex. [b] Total energy of the DTAc in the complex. [c] Energy of the DTAc−DNA interaction decomposed in van der Waals (vdw) and electrostatic (elec) terms. [d] Total energy of the complex: $E_{DNA} + E_{DTAc} + E_{DTAc-DNA}$.

Hoogsteen model obtained with the diaminopurine base and by replacing the NH_2-2 amino group by hydrogen. The best corresponding structure is shown in Figure S8 (Supporting Information). The DNA in the major 1/1 ATAc−DNA complex adopts approximately the same conformation as in the major 1/1 DTAc−DNA (rmsd for heavy atom of 1.4 Å) (Figure S9, Supporting Information).

ATAc and DTAc as Nuclease Mimics and Cleaving Agents at Abasic Sites. A number of molecules have been shown to cleave abasic sites at low doses (Behmoaras *et al.*, 1981; Pierre & Laval, 1981; Male *et al.*, 1982; Malvy *et al.*, 1986; Vasseur *et al.*, 1987). We prepared series of molecules in which an intercalator is linked to a nucleic base through chains of different length and nature. Among all the molecules described, DTAc and ATAc proved to be the most efficient cleaving agent (Fkyerat *et al.*, 1993a), being more active than the prototypical Lys-Trp-Lys tripeptide by several orders of magnitude in terms of the concentrations required to obtain comparable cleavage ratios (Fkyerat *et al.*, 1993a). DTAc and ATAc were engineered according to Scheme 2 in which each constituting moiety is designed for a specific function. We postulated different modes of binding of the drugs to the abasic DNA, including modes in which the base and the intercalator either stack intramolecularly in the abasic site (A) or intercalate and dock in the abasic site with the chromophores being separated by one or two base pairs (B). All cleavage data obtained are in accordance with these postulated schemes. However, no direct proof of the mode of interaction could be obtained concerning notably the postulated key role of the base in the complex. The present study yields an unequivocal answer. The two drugs DTAc and ATAc bind selectively to the abasic site. (1) The aminochloromethoxyacridine is a well-known DNA intercalator devoid of any noticeable base-sequence selectivity. Thus, the abasic undecamer studied possesses ten possible intercalation sites. However, the acridine ring in both DTAc and ATAc intercalates quite selectively at one single site between the C3·G20 and A4·T19 base pairs (with the restriction of the limits of the NMR technique to detect any other possible complex present in very minor proportions). In addition, it is interesting to note that the single difference between the major and the minor complexes for both drugs resides in the 180° rotation of the acridine ring around the Acr-C9−N11 bond within the same intercalation site. (2) The base docks inside the abasic site pocket, most probably forming a Hoogsteen type base pair with the complementary thymine that faces the abasic site. Like an anchor, the base moiety in both DTAc and ATAc controls the positioning of the intercalator both in terms of distance, two base pairs away, and in terms of DNA polarity, on location the 5′-side versus the 3′-side. (3) The linking chain lies in the minor groove as hypothesized in the original scheme, a situation that is probably energetically favored for each constituting moiety of the molecules. Polyamines in general preferentially bind in the minor groove (Schmid & Behr, 1991); 9-aminoacridines intercalate in DNA with the 9-amino function, which is the point of attachment in DTAc and ATAc, protruding in the minor groove (Woodson & Crothers, 1988), while N9 of adenine or diaminopurine faces the minor groove preferentially if paired to the complementary thymine in the Hoogsteen mode. Furthermore, docking of the base at the abasic site directs intercalation of the acridine ring to the 5′-side, a situation that avoids overcrowding and destabilizing steric effects as indicated by modeling in the alternate 3′-side intercalation complex. All the data are in favor of a unique binding mode that is energetically favored. Binding of the drug leads to an increase in the melting temperature of 15 °C. We have shown that in the absence of any drug the abasic undecamer forms a kink of about 30° (Coppel *et al.*, 1997). In the presence of DTAc and ATAc, no kinking could be detected. However, experimental data do not allow definitive conclusions.

Molecules DTAc and ATAc have been designed as mimics for AP endonucleases of the AP lyase type that cleave abasic sites by a β-elimination reaction. This comparison holds in terms of cleavage efficiency as the substrate DNA is cleaved at nanomolar concentrations. The DTAc−undecamer complex examined can thus be viewed as a good model for the "enzyme−substrate" complex inside which the reaction takes place. The cleavage reaction requires the presence of a basic function in the vicinity of the abasic site (Scheme 2). The polyamino linker fulfills the role. The p*K*'s of the different amino groups in DTAc have been determined and discussed in a previous study (Belmont *et al.*, 1996). Three protonation sites have been determined corresponding to p*K*'s of 9.8, 8.1, and 6.7 (in addition to p*K*'s of 4.0 that correspond to protonation of the diaminopurine ring, a process that cannot intervene at the neutral pH of this study). Although the p*K*'s are affected in a nonpredictable manner when DTAc is complexed with DNA, the active form of DTAc at pH 7.0 is most probably the species in which the aminoacridine (protonated on the ring as usual for 9-aminoacridines) and one nitrogen of the linker are essentially protonated, while the other nitrogen of the linker is essentially unprotonated. The protonated nitrogen of the linker participates in binding the drug to DNA by ionic interactions with the phosphates. The unprotonated nitrogen participates in the reaction by catalyzing strand cleavage. Indeed, one feature that emerges from the modeling study is the positioning of the DTAc-N7 nitrogen atom which is sufficiently close to the abasic site (Figure 7) to react with the open chain aldehydic form (Scheme 1) either by abstracting the 2′-hydrogen (DTAc-N7−X6-H2′ distance of 4.12 Å in the Hoogsteen model) or by forming an immonium intermediate (DTAc-N7−X6-C1′ distance of 4.40 Å in the Hoogsteen model), thus catalyzing the cleavage via β-elimination. The present study cannot give any indication in favor of either of these two possible modes of catalysis. DTAc and ATAc can thus be viewed as AP lyase mimics since they recognize quite selectively the abasic DNA as substrate, and in the preformed complex, the catalytic amino functional group of the mimic is correctly positioned to trigger the cleavage reaction. These features constitute good evidence for interpreting the extremely high cleavage efficiency of the DTAc molecule.

As noted in the accompanying paper (Coppel *et al.*, 1997), abasic sites and single-base bulges present some analogies in that one polynucleotide strand must accommodate an extra

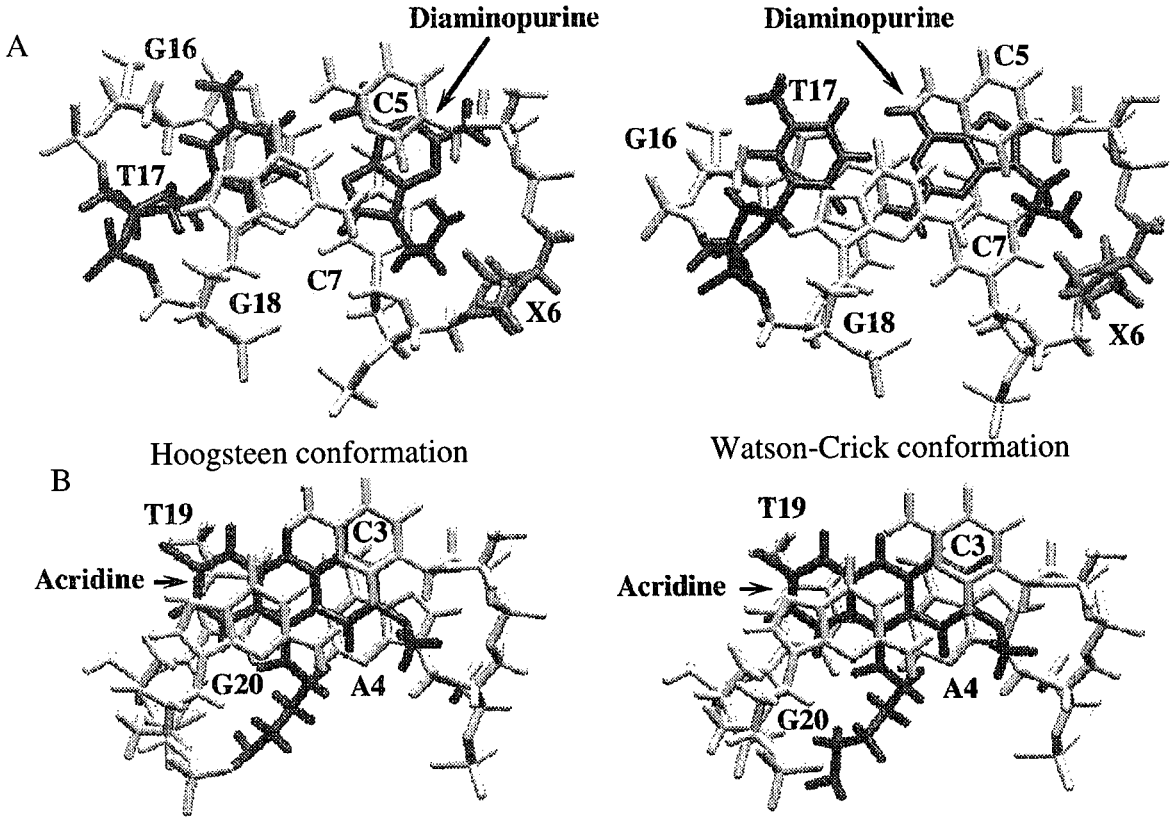

FIGURE 6: View looking down to the helical axis for the Hoogsteen and Watson−Crick models. The AP site (X6), the opposite T17 residue, and the diaminopurine are shown in darkened bonds. (A) Position of the diaminopurine ring in the abasic pocket. (B) Position of the acridine ring between the C3·G20 and A4·T19 base pairs. Note that the diaminopurine stacks better with the C7 residue in the Hoogsteen model than in the Watson−Crick model.

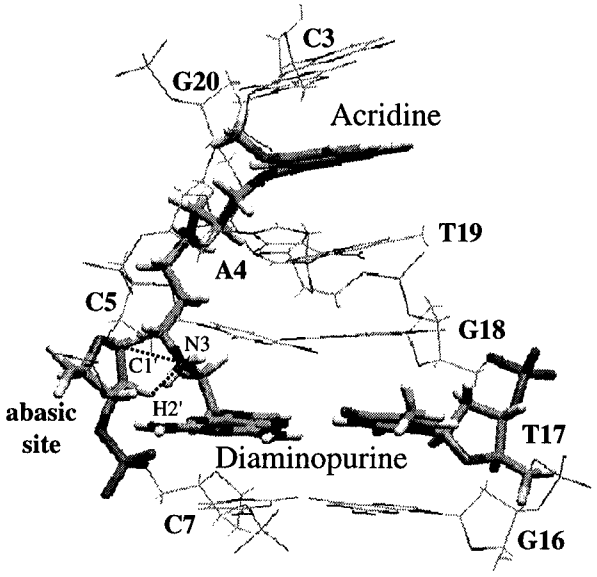

FIGURE 7: Structure of the d($C_3A_4C_5X_6C_7$)·d($G_{16}T_{17}G_{18}T_{19}G_{20}$) region of the Hoogsteen model. The abasic site and DTAc are displayed as sticks. Note the proximity of the DTAc-N3 atom and the O4′ and the H2′ atoms of the abasic site (3.32 and 4.56 Å, respectively).

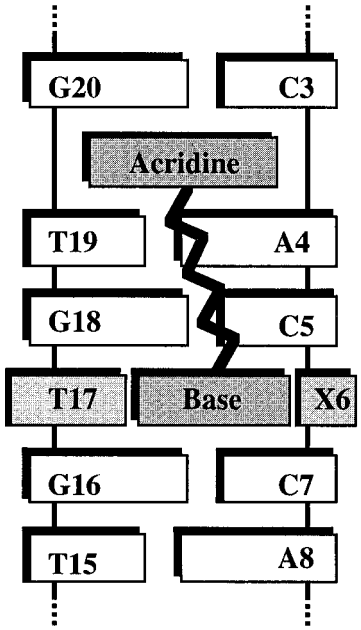

FIGURE 8: Schematic representation of the 1/1 DTAc−DNA and 1/1 ATAc−DNA complexes.

base, which has been shown to be located either inside or outside the helix depending notably on the nature of the base involved and on its flanking sequences. We previously reported (Wilson *et al.*, 1994) a study of the interaction of the molecules DTAc and ATAc with synthetic RNA single-base bulge duplexes. T_m measurements of RNA bulged duplex in the presence or in the absence of ATAc and DTAc (Wilson *et al.*, 1994) showed that DTAc and ATAc stabilize an A-bulge RNA octamer (by 21.0 and 9.0 °C, respectively) and a U-bulge RNA octamer (by 21.8 and 6.8 °C, respectively). These results imply that DTAc and ATAc have significant interaction with a U bulge as expected but surprisingly also interact strongly with an A bulge, illustrating the complexity of the interaction of such drugs with nucleic acids.

Conclusion. We have used two-dimensional NMR experiments and molecular modeling calculations to show that DTAc and ATAc act in a very similar fashion. They bind exclusively in the C3·G20−C7·G16 region with the acridine

ring intercalating between the C3·G20 and A4·T19 base pairs, the linker positioning in the minor groove, and the base moiety docking into the abasic site (X6). The results obtained in this study are in accordance with the general hypothesis and scheme as postulated. (a) The intercalator moiety stabilizes the complexation of molecule DTAc and ATAc with DNA. (b) The base moiety recognizes and inserts into the pocket created by the missing base. (c) The amino protons of the linking chain can form hydrogen bonds with DNA and stabilize the complex by electrostatic interactions. Furthermore, an amine of the chain is sufficiently close to the abasic site for cleavage activity. It can thus be concluded that molecules DTAc and ATAc possess the adequate structural elements required to interact specifically and efficiently with an abasic site. In addition to providing the structural data to account for the extreme cleavage activity of the DTAc and ATAc molecules, the present study furnishes a structural basis for engineering new molecules for recognizing the important and numerous abasic DNA lesions and possibly interfering with their repair processes.

ACKNOWLEDGMENT

We acknowledge C. Maerschalk and Professor J. Reisse (Université Libre de Bruxelles) for assistance with NMR spectroscopy (600 MHz NMR machine) and for fruitful discussions. We thank Professor R. Lavery for critical reading of the manuscript.

SUPPORTING INFORMATION AVAILABLE

Three tables listing the proton chemical shifts for (1) the acridine moiety in the minor 1/1 DTAc−DNA complex, (2) the acridine moiety in the major 1/1 ATAc−DNA complex, and (3) the DNA in the major 1/1 ATAc−DNA complex, and nine figures showing (1) the comparison between the 250 ms NOESY experiment realized with the C8-H and C8-^{2}H of DTAc, (2) the aromatic region of the one-dimensional NMR spectra, (3) the expanded region of the 250 ms NOESY and (4) of the 60 ms TOCSY spectra of the 1/1 ATAc−DNA complex in D_2O at 10 °C, (5) the superposition of the DNA from the Hoogsteen and Watson−Crick models, (6) the model for the minor complex in the Hoogsteen conformation, (7) the model with the acridine ring intercalated between the A8·T15 and C9·G14 base pairs, (8) the model for the major 1/1 ATAc−DNA complex in the Hoogsteen conformation and (9) the superposition of the DNA from the model for the 1/1 DTAc−DNA and 1/1 ATAc−DNA complexes in the Hoogsteen conformation (12 pages). Ordering information is given on any current masthead page.

REFERENCES

Arnott, S., Chandrasekaran, R., Birdsall, D. L., Leslie, A. G. W., & Ratliff, R. L. (1980) *Nature (London) 283*, 743−745.
Bailly, V., & Verly, W. (1989) *Nucleic Acids Res. 17*, 3617−3618.
Behmoaras, T., Toulme, J. J., & Helene, C. (1981) *Nature (London) 292*, 858−859.
Belmont, P., Boudali, A., Constant, J.-F., Demeunynck, M., Fkyerat, A., Lhomme, J., Michon, P., & Serratrice, G. (1997) *New J. Chem. 21*, 47−54.
Berthet, N., Boudali, A., Constant, J.-F., Decout, J.-L., Demeunynck, M., Fkyerat, A., Garcia, J., Laayoun, A., Michon, P., & Lhomme, J. (1994) *J. Mol. Recognit. 7*, 99−107.
Boiteux, S., & Laval, J. (1982) *Biochemistry 21*, 6746−6751.
Chazin, W. J., Rance, M., Chollet, A., & Leupin, W. (1991) *Nucleic Acids Res. 19*, 5507−5513.
Chollet, A., & Kawashima, E. (1988) *Nucleic Acids Res. 16*, 305−317.
Constant, J.-F., O'Connor, T., Lhomme, J., & Laval, J. (1988) *Nucleic Acids Res. 16*, 2691−2703.
Constant, J.-F., Fkyerat, A., Demeunynck, M., Laval, J., O'Connor, T. R., & Lhomme, J. (1990) *Anti-Cancer Drug Des. 5*, 59−62.
Coppel, Y., Berthet, N., Constant, J.-F., Coulombeau, C., Coulombeau, Ce., Garcia, J., & Lhomme, J. (1997) *Biochemistry 36*, 4817−4830.
Demple, B., & Harrison, L. (1994) *Annu. Rev. Biochem. 63*, 915−948.
Feigon, J., Leupin, W., Denny, W. A., & Kearns, D. R. (1983) *Biochemistry 22*, 5943−5951.
Fkyerat, A., Demeunynck, M., Constant, J.-F., Michon, P., & Lhomme, J. (1993a) *J. Am. Chem. Soc. 115*, 9952−9959.
Fkyerat, A., Demeunynck, M., Constant, J.-F., & Lhomme, J. (1993b) *Tetrahedron 49*, 11237−11252.
Giessner-Prettre, C., & Pullman, B. (1976) *Biochem. Biophys. Res. Commun. 70*, 578−581.
Goulaouic, H., Carteau, S., Subra, F., Mouscadet, J. F., & Auclair, C. (1994) *Biochemistry 33*, 1412−1418.
Lavery, R., & Sklenar, H. (1988) *J. Biomol. Struct. Dyn. 6*, 63−91.
Lavery, R., & Sklenar, H. (1989) *J. Biomol. Struct. Dyn. 6*, 655−667.
Lavery, R., & Sklenar, H. (1990) *CURVES 3.0., Helical Analysis of Irregular Nucleic Acids*, Laboratory for Theoretical Biochemistry, CNRS, Paris.
Lavery, R., Zakrzewska, K., & Sklenar, H. (1995) *Comput. Phys. Commun. 91*, 135−158.
Lindahl, T. (1993) *Nature (London) 362*, 709−715.
Loeb, L., & Preston, B. (1986) *Annu. Rev. Genet. 20*, 201−230.
Male, R., Fosse, V., & Kleppe, K. (1982) *Nucleic Acids Res. 20*, 6305−6308.
Malvy, C., Prevost, P., Gansser, C., & Paelotti, C. (1986) *Chem.-Biol. Interact. 57*, 41−53.
Manoharan, M., Ransom, S. C., Mazumder, A., Gerlt, J. A., Wilde, J. A., Withka, J. M., & Bolton, P. H. (1988a) *J. Am. Chem. Soc. 110*, 1620−1622.
Manoharan, M., Mazumder, A., Ransom, S. C., Gerlt, J. A., & Bolton, P. H. (1988b) *J. Am. Chem. Soc. 110*, 2690−2691.
Mazunder, A., Gerlt, J. A., Absalon, M. J., Stubbe, J., Cunnigham, R. P., Withka, J., & Bolton, P. H. (1991) *Biochemistry 30*, 1119−1126.
Millican, T. A., Mock, G. A., Chauncey, M. A., Patel, T. P., Eaton, M. A., Gunning, J., Cutbush, S. D., Neidele, S., & Mann, J. (1984) *Nucleic Acids Res. 12*, 7435−7453.
Pierre, J., & Laval, J. (1981) *J. Biol. Chem. 256*, 10217−10220.
Scheek, R. M., Russo, N., Boelens, R., Kaptein, R., & Van Boom, J. H. (1983) *J. Am. Chem. Soc. 105*, 2914−2916.
Schmid, N., & Behr, J.-P. (1991) *Biochemistry 30*, 4357−4361.
Takeshita, M., Chang, C.-N., Johnson, F., Will, S., & Grollman, A. P. (1987) *J. Biol. Chem. 262*, 10171−10179.
Vasseur, J. J., Rayner, B., Imbach, J. L., Verna, S., McCloskey, J. A., Lee, M., Chang, D. K., & Lown, J. L. (1987) *J. Org. Chem. 52*, 4994−4998.
Wallace, S. S. (1988) *Environ. Mol. Mutagen. 12*, 431−477.
Wilde, J. A., Bolton, P. H., Mazumder, A., Manoharan, M., & Gerlt, J. A. (1989) *J. Am. Chem. Soc. 111*, 1894−1896.
Wilson, W. D., Ratmeyer, L., Cegla, M. T., Spychala, J., Boykin, D., Demeunynck, M., Lhomme, J., Krishnan, G., Kennedy, D., Vinayak, R., & Zon, G. (1994) *New J. Chem. 18*, 419−423.
Woodson, S. A., & Crothers, D. M. (1988) *Biochemistry 27*, 8904−8914.
Wüthrich, K. (1986) *NMR of Proteins and Nucleic Acids*, pp 203−255, John Wiley & Sons, New York.

BI962678Q